Geophys. Astrophys. Fluid Dynamics, Vol. 66, pp. 101–131
Reprints available directly from the publisher
Photocopying permitted by license only

THE STABILITY OF STRATIFIED JETS

B. R. SUTHERLAND and W. R. PELTIER

Department of Physics, University of Toronto, Toronto, Ontario, Canada M5S 1A7

(Received 9 September 1991; in final form 15 February 1992)

We study numerically the two dimensional linear instabilities of an incompressible, inviscid, density stratified, symmetric jet as a function of a width parameter, D. In the limit of infinite D, the maximum growth rate of temporal instability exponentially approaches that of the shear flow on either flank of the jet. The growth rate need not approach this limit monotonically, however. For some stratified flows it is possible that the odd (varicose) mode of a jet with sufficiently large width may grow more rapidly than the even (sinuous) mode. We also examine spatiotemporal instabilities of the Bickley profile, focusing specifically upon the identification of the regime of parameter space in which the flow is absolutely or convectively unstable. Finally, our methods of spatiotemporal linear stability analysis are applied to a more realistic asymmetric jet which mimics the internal wave related flow that develops in the lee of a topographic obstacle when "breaking" occurs. This analysis appears to bear strongly upon the interaction that occurs subsequent to wave breaking that leads to intense wave, mean-flow interaction.
KEY WORDS: Jets, stability, stratification.

1. INTRODUCTION

Significantly increased understanding of the complex dynamics of interacting vortices has been forthcoming recently through the application of large eddy resolving numerical integration techniques. Such phenomenology is observed experimentally in mixing layers (Overman and Zabusky, 1982; Flierl *et al.*, 1983) and of course occurs naturally in the large scale jet-like flows of the Earth's atmosphere and, perhaps most notably, in the zonal shear bands that dominate the atmospheres of Jupiter and Saturn. Recent numerical analyses of the dynamics of vortex interaction have revealed a wide range of interesting processes including vortex merging and stability of vortices in surrounding turbulence (Marcus, 1990) of which the Red Spot of Jupiter is a classical example.

Because the stability and evolution of interacting vortices depends sensitively on their extent and separation, and because the symmetric jet with width as parameter provides an ideal setting for the examination of such effects, we have initiated a detailed program of study of such flows. In this initial paper, we focus upon the linear stability of small scale inviscid stratified flow. Our work on symmetric jets builds upon the foundations laid by Drazin and Howard (1966) who found analytic solutions for temporal instability of various jet profiles. In flows that are unstratified and have a piecewise-linear horizontal velocity profile, analytic solutions can be found for linearly unstable modes of any wavenumber. Although in general such flows are not physically realizable, analysis of them and particularly of the symmetric trapezoidal jet, may provide useful indications of the basic structure of jet instabilities. We comment briefly on the stability of the trapezoidal jet in the beginning of Section 3. We examine in detail, thereafter, a flow whose basic state velocity profile has the

Bickley [$\mathrm{sech}^2(z)$] form (Bickley, 1937). This particular flow has the advantage that it adequately approximates realizable experimental jet profiles more accurately (Sato, 1960; Sato and Kuriki, 1961), and that numerical results can be compared with analytic solutions which are known for the curve of marginally stability (Drazin and Howard, 1966).

It is well known that symmetric jets support the development of two modes of instability: even (sinuous) modes give rise to a streamline pattern in which the propagating modes developing in each shear zone of the jet travel in phase; odd (varicose) modes, on the other hand, are characterized by a streamline pattern that periodically pinches and broadens since the propagating modes in adjacent shear zones are 180° out of phase. For the Bickley profile, unstable even modes exist only when $J < J_c^e \simeq 0.127$ and unstable odd modes exist only when $J < J_c^o \simeq 0.109$, where J is the Bulk Richardson Number that provides a dimensionless measure of the ratio of the stabilizing effect of the density stratification to the destabilizing effect of the shear (Drazin and Howard, 1966). The constraints on J cited above are in accordance with the Miles-Howard Theorem (Miles, 1961) which asserts that no instabilities can exist in a stratified shear flow if $J > 1/4$ everywhere in the flow domain.

The first comprehensive numerical analysis of the linear temporal instability of inviscid stratified flows was performed by Hazel (1972), who, in his study of the Bickley profile, calculated the growth rates of the most unstable even temporal modes (MTE) and of the most unstable odd temporal modes (MTO) for various degrees of stratification. He found that, in any stratified fluid, MTE modes always develop more rapidly than MTO modes, the former having a greater wavenumber and smaller phase speed. Generally, it is not always true that the MTE mode is the dominant mode of instability. As we report below, our analyses of the symmetric jet demonstrate that the MTO mode may grow more quickly in stratified jets that are sufficiently wide. Some insight into the mechanism involved is provided through an investigation of the Reynolds stress and vertical density flux profiles that characterize the two modes of instability. Briefly, we find that the MTO mode extracts kinetic energy more efficiently from the mean flow of a wide jet than from the mean flow of a jet of smaller width. The corresponding efficiency of the MTE mode does not vary greatly with the jet width.

A modern theoretical analysis of the stability of jet flows would not be complete without some effort to understand the nature of spatiotemporal disturbances. Such modes, characterized generally by a complex valued wavenumber, arise naturally in experiments which are inherently spatially non-uniform (such as those that employ a plate to enforce a wake in the inflow), and they can dominate the unstable behaviour observed in jets and wakes. Experiments that attempt to simulate the dynamics of jets such as the laterally homogeneous zonal flows in planetary atmospheres (for example, the work by Sommeria *et al.* 1988) may not adequately represent the spatiotemporal disturbances that occur in the natural system of interest. For this reason, we will also include in this paper an analysis of the time asymptotic evolution of a wavepacket with fixed (real) group velocity, C. Special cases of such disturbances are wavepackets centered about the mode of maximum temporal growth and wavepackets centered about the mode of maximum spatial growth. The evolution of

the wavepacket as observed in a frame of reference moving with velocity C (so that the wavepacket has zero group velocity in this frame) determines the absolute/convective instability of the flow. For a flow that is convectively unstable in this frame, spatial disturbances that arise will be "convected" downstream away from the observer. Conversely, flows which are absolutely unstable amplify the wavepacket so that eventually it will perturb all points of the flow.

The theory of the development of spatiotemporal instability has been successfully applied to the interpretation of simple experiments such as those performed by Sato and Kuriki (1961) who observed the amplification of spatially growing modes in a background flow whose velocity profile they described in theory by a gaussian curve. The first detailed study of spatiotemporal instabilities of a jet was performed by Betchov and Criminale (1966) who numerically computed growth rates for the unstratified Bickley jet and wake. A surprising result of their analysis was the presence of hyperbolic singularities in the wavenumber as a function of phase speed. They suggested that interesting dynamics may arise in flows with spatially growing modes that pass through one of these singularities. In the unstratified Bickley jet, the neutral modes that travel with phase speed 1.06 may exhibit such peculiar behaviour. A detailed numerical analysis of spatiotemporal disturbances was performed by Zabusky and Deem (1971) who integrated the incompressible Navier Stokes equations directly. They were able to simulate the spatial growth of instabilities of a Bickley jet and of a flow with a gaussian velocity profile. Their studies of the first stages of instability agree well with the results of linear stability analysis.

The distinction between absolute and convective instability in fluids was clearly identified by Briggs (1964) and Bers (1973) in work directed towards the understanding of the spatiotemporal growth of wavepackets with zero group velocity that arise in plasma physics. Only recently have their ideas been applied to classical fluid motion, however. Absolute/convective instability of an unstratified hyperbolic tangent shear layer has been analyzed by Heurre and Monkewitz (1985) and of the stratified shear layer by Lin and Pierrehumbert (1987)[1]. Because of the symmetric nature of the velocity profile employed, both analyses demonstrated the flow to be absolutely unstable when monitored by an observer travelling within a range of velocities about zero relative to the velocity of the vertical mid-point of the flow. This range was shown to decrease as stratification increases, emphasizing the stabilizing nature of the stratification. No corresponding analysis has been performed for the stratified (or unstratified) jet.

In Section 2, we review a number of theorems concerning the linear instability of a stratified, inviscid, incompressible flow. The numerical techniques employed to solve the Taylor-Goldstein equation for the temporal and spatiotemporal problem are discussed with special attention to the accuracy of the solutions. We are able to test some of our results by comparing them with analytic solutions and with quantities previously computed numerically, such as the maximum growth rates calculated by Hazel and the spatiotemporal amplification rates calculated by Betchov and

[1] Note, the bulk Richardson number in Figure 2 of Lin and Pierrehumbert should be $J = 0.05$ instead of $J = 0.20$.

Criminale. In Section 3, we examine how the maximum growth rates modify as a function of jet width. In this way, the effect of interference between linearly developing, oppositely oriented vortices can be studied as they separate. We find that the growth rate is not necessarily a monotonic function of the jet width. Such behaviour we attempt to understand by comparing the variations in Reynolds stress and vertical density flux profiles and by involving the ideas of over-reflection theory. We briefly discuss the theory of absolute and convective instability in Section 4. We show that wavepackets centered about the mode of maximum temporal growth (MT) and the mode of maximum spatial growth (MS) have a real valued group velocity and, therefore, frames of reference exist in which these modes may give rise to absolute instability. In particular, the wavepacket centered about the MT mode has the largest growth rate of all wavepackets with respect to a moving frame of reference. Thus we explain how this mode is the one frequently observed in experiments. In our examination of symmetric jets, we study the absolute/convective instability of the Bickley jet with varying degrees of stratification, specifying for even and odd modes the range of reference frame speeds over which the flow is absolutely unstable.

The techniques we use to study the spatiotemporal instability of symmetric jets are easily extended to more general flows. In Section 5, we perform a linear stability analysis of a jet whose non-linear evolution was studied by Scinocca and Peltier (1991). The jet, which they used to study the origins of downslope windstorm pulsations, is asymmetric in the vertical profiles of horizontal velocity and Brunt Väisälä frequency. The lower boundary of the jet is fixed and the upper boundary radiates energy outward. Our analysis of the temporal instability of the jet shows that the MT mode has the same wavelength and group velocity as observed in the initial stages of instability of the non-linear numerical simulation of Scinocca and Peltier. The jet gives rise to eddies of opposite vorticity which, as it turns out, are qualitatively similar to the odd mode of instability that develops in the symmetric jet. Unlike the instabilities of the symmetric jet, however, the instability that develops in this jet is not localized to the shear zone, but the kinetic energy which it extracts from the mean flow is continuously radiated upwards. Studying spatial modes of instability, we find that the MS mode has a wavelength which is greater than twice the wavelength of the MT mode. Therefore, Gaster's relationship (Gaster, 1962) between the spatial and temporal growth rates of disturbances with the same wavelength is not applicable. Like the MT mode, the MS mode is non-local and the magnitude of the perturbation decreases vertically upward less quickly than the temporal mode. Finally, we determine the absolute/convective instability of the jet when observed in a frame moving with a constant horizontal velocity, C. We discover that the flow is absolutely unstable for small positive values of C and we confirm empirically that the MT mode corresponds to the wavepacket with the largest growth rate.

2. THEORETICAL PRELIMINARIES

A flow with velocity profile $U = U(z)$ and density $\rho = \rho(z) = {}_0\exp[-\sigma\beta(z)]$ may give rise to the growth of unstable fluctuations. In the Boussinesq limit, linear

instability analysis of stratified, incompressible, inviscid fluid defines fluctuations of velocity, pressure, and density by perturbations, denoted by $\vec{u}'$, p', and ρ' respectively, which are superimposed on the background flow. By Squire's Theorem, any instability initially grows as a two dimensional disturbance (for example, see Smyth and Peltier, 1989). Hence it is possible, through a change of variables, to express the x and z component of the perturbed velocity in terms of derivatives of a stream function $\psi(x, z)$. The disturbance is assumed to be periodic in the direction of flow allowing ψ to be resolved into Fourier components with horizontal wavenumber α and phase speed c and with amplitude that varies with z. Explicitly, $\psi(x, z) = \phi(z)\exp[i\alpha(x - ct)]$. Substituting these quantities into the basic equations of motion and keeping only lowest order terms, we find that the amplitude, $\phi(z)$, must satisfy the classical Taylor-Goldstein equation:

$$\phi'' - \eta^2\phi = 0, \tag{1}$$

where

$$\eta^2 = \frac{-N^2}{(U-c)^2} + \frac{U''}{(U-c)} + \alpha^2. \tag{2}$$

N is the Brunt-Väisälä frequency, defined by $N^2 = g\sigma\beta'(z)$. In our study of symmetric jets we consider the case where N^2 is constant, corresponding to exponentially density stratified fluid. However, N^2 is generally a function of z as is the case in our examination of a non-symmetric jet in Section 5. The local (gradient) Richardson number is $\mathrm{Ri}(z) = N^2/[U'(z)]^2$. If z_s is an inflexion point of background flow $[U''(z_s) = 0]$, the bulk Richardson number is defined by $J = \mathrm{Ri}(z_s)$. For the Bickley jet, $J = 3\sqrt{3}N^2/4$.

Given a specific value of α, the Taylor-Goldstein equation poses an eigenvalue problem in which the eigenfunction is ϕ and the eigenvalue is c. Both α and c are generally complex variables ($\alpha = \alpha_r + i\alpha_i$ and $c = c_r + ic_i$) and the product $\omega = \alpha c$ is defined to be the complex frequency whose real part (ω_r) is the frequency of the instability and whose imaginary part (ω_i) is the exponential growth rate.

It is usual to assume that c is an analytic function of α. For the unstratified Bickley jet this has been previously verified numerically by Betchov and Criminale (1966). In Figure 1 we show the values of the complex wavenumber as a function of phase speed for even modes of stratified flow with $N^2 = 0.025$. The lines correspond to constant values of α_r and α_i. From top to bottom α_r ranges from 0.6 to 2.0 in steps of 0.1 and from left to right α_i ranges from -0.9 to 2.0. In particular, the bold line corresponds to temporal modes, for which $\alpha_i = 0$. Because these lines intersect at right angles we see that c (and hence ω) is an analytic function of α. It is interesting to observe in Figure 1 the presence of a hyperbolic singularity in the complex plane near $c = 0.38 + i0.15$. As noted by Betchov and Criminale, a singularity of this kind may give rise to interesting dynamics for unstable modes with wavenumbers in its proximity.

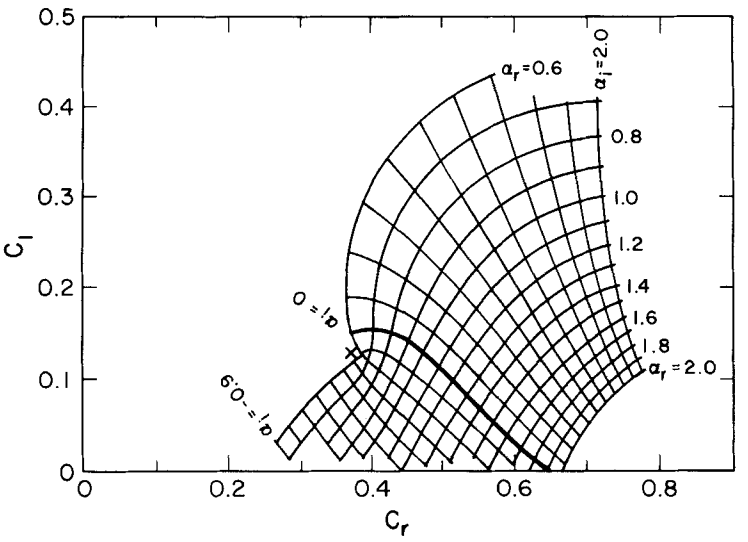

Figure 1 Complex wavenumber as a function of phase speed for the stratified Bickley jet with $N^2 = 0.025$.

There are three different modes of instability which are of interest. Modes for which $\alpha = \alpha_r$ is real and ω_i is positive, are temporally unstable and grow exponentially in time. Modes for which $\omega = \omega_r$ is real and α_i is negative, are spatially unstable and grow exponentially in space though no growth occurs in time at a fixed position. Finally, in the context of absolute/convective instability, we are interested in modes corresponding to wavepackets with real-valued group velocity. Details of the theory of such instability are presented in Section 4.

Modes with the largest growth rate are examined in detail since these will dominate the non-linear dynamics of the flow that ensues. We define the MT mode as the temporal mode with the largest growth rate, ω_i, as a function of α_r. (In our consideration of symmetric jets, there are two such modes, denoted by the MTE and MTO modes, which correspond to the fastest growing even and odd modes, respectively.) The spatial mode with the largest growth rate, $-\alpha_i$, as a function of ω_r we refer to as the MS mode. For a wavepacket with (real) group velocity C, we refer to the MC mode as the wavepacket with the largest growth rate, ω_i^C as a function of C. This last definition, as we will show in Section 4, is superfluous since the MC mode corresponds exactly with the MT mode.

All of the results to be described here are based upon calculations performed on an IBM RISC 6000 computer. The Taylor-Goldstein equation is integrated using a shooting method similar to that described by Hazel (1972) with the following differences. The integration proceeds using a fourth order Runga-Kutta-Nyström method, an algorithm based on an ODE solver, ERNY (Sharp and Fine, 1987), which is optimized to efficiently integrate equations of the form $\phi'' = A\phi$. Boundary conditions are imposed by assuming that $\phi(z) \simeq \exp(-\eta z)$ at a small value of $z = -z_{\max}$, where η is the complex square root (uniquely defined as the branch with

positive real part) of the coefficient of ϕ in the Taylor-Goldstein equation, defined by equation (2). The Taylor-Goldstein equation is integrated from $-z_{\max}$ to $z_{\max}$ and the value of $W(c) = \phi' + \eta\phi$ evaluated at $z = z_{\max}$ is made to converge to zero by the successive choices of c. When the flow is symmetric, even modes are found by ensuring that ϕ has the same sign at $z = -z_{\max}$ and $z = z_{\max}$; odd modes are found by ensuring that ϕ has the opposite sign at each boundary. Each guess to determine the correct eigenvalues is improved quadratically by using a complex inverse parabolic zero-finding method: three values of $[c, W(c)]$ are used to find the coefficients of the equation $c = a_2 W^2 + a_1 W + a_0$, and so the next best guess to the zero of W is $c = a_0$. In tests, this approach was generally faster and more reliable than Muller's (parabolic) method (Muller, 1956).

The value of $z_{\max}$ requires some attention. If it is too large then $\phi(z_{\max})$ may be so close to zero that integration will give only the zero solution. Conversely, if $z_{\max}$ is too small, the assumption that η is approximately constant may be invalid. Keeping the largest exponential terms in the asymptotic expansion of η^2 for the Bickley jet, we find

$$\eta^2 \simeq -\frac{N^2}{c^2} + \alpha^2 + \frac{6}{c} e^{-4z}.$$

When $z_{\max} \simeq 5$ and if c is of order 0.1, the assumption that η is constant is accurate to 7 digits. It may be necessary to increase the value of $z_{\max}$ if α and N^2 are small. However, unavoidable numerical errors arise when α is too close to zero. This problem turns out to be of little concern since we are interested primarily in the wavenumbers which give maximium growth, where α is significantly large.

In practice, it is sufficient to assume convergence has been achieved when the norm of W is less than a small number, ε. Typically, for $\varepsilon = 10^{-8}$, six digit accuracy of the eigenvalues is assured. The accuracy of the eigensolution is tested by checking its sensitivity to the values of $z_{\max}$, the integration step size, and ε.

3. TEMPORAL INSTABILITIES OF SYMMETRIC JETS

The majority of our work on linear temporal instabilities focuses on a density stratified jet whose basic state has the Bickley profile, which hereafter we refer to as a "smooth jet". In order to increase our understanding of the instabilities in a smooth jet, we begin by presenting analytic results for a symmetric trapezoidal jet in unstratified fluid.

The trapezoidal velocity profile of width D has the form,

$$\mathscr{U}_D(z) = \begin{cases} 1, & |z| \leqslant D, \\ D + 1 - |z|, & D + 1 > |z| > D, \\ 0, & |z| \geqslant D + 1. \end{cases} \tag{3}$$

Because the trapezoid is piecewise-linear, the solutions of the Taylor-Goldstein equation when $N^2 = 0$ are of the form $\phi(z) = \mathscr{C}_- \exp(-\alpha z) + \mathscr{C}_+ \exp(\alpha z)$ over each linear segment of the velocity profile. Vanishing boundary conditions are imposed at $z = \pm\infty$ and matching conditions at points where the derivative of U_D is discontinuous are defined so that the pressure, $(U_D - c)\phi' - U_D'\phi$ and the normal velocity, $\phi/(U_D - c)$, are continuous (see Drazin and Reid, 1981, p. 144). Thus we obtain the eigenvalue relation:

$$0 = (4\alpha^2)c^2 - 2\alpha c[2\alpha \mp e^{-2D\alpha}(1 - e^{-2\alpha})] + \{-1 + 2\alpha + e^{-2\alpha} \mp e^{-2D\alpha}[1 - (1 + 2\alpha)e^{-2\alpha}]\}, \tag{4}$$

where the upper (lower) sign corresponds to the even (odd) mode. From this equation, it is a simple matter to find numerically the growth rates of temporal modes of instability.

The limit of infinite D corresponds to the left-hand shear[2]:

$$\mathscr{U}_D(z) = \begin{cases} 1, & z \geqslant 1, \\ z, & 0 < z < 1, \\ 0, & z \leqslant 0. \end{cases} \tag{5}$$

Instabilities of the shear obey the eigenvalue relation that is the infinite D limit of (4). The equation solved for c is

$$c = \tfrac{1}{2}\{1 \pm \alpha^{-1}[(\alpha - 1 - e^{-\alpha})(\alpha - 1 + e^{-\alpha})^{1/2}\} \tag{6}$$

The shear is unstable to modes with wavenumbers $0 \leqslant \alpha \leqslant \alpha_{\max}$ where $\alpha_{\max} \simeq 1.2785$ is the solution of $\alpha - 1 - \exp(-\alpha) = 0$. The most unstable mode has wavenumber α_0 such that the maximum growth rate,

$$\omega_i^{\max} = \alpha_0 c_i = \tfrac{1}{2}[-(\alpha_0 - 1 - e^{-\alpha_0})(\alpha_0 - 1 + e^{-\alpha_0})]^{1/2},$$

is largest for $0 \leqslant \alpha_0 \leqslant \alpha_{\max}$. Explicitly, $\alpha_0 \simeq 0.7968$ and $\omega_i^{\max} \simeq 0.2012$. Hereafter, the value of the maximum growth rate of unstable modes that develop in the shear will be referred to as the "shear limit".

The maximum growth rate of even and odd modes of instability are plotted as a functon of jet width in Figure 2. Both rates are within one percent of the shear limit when $D > 2.5$. No odd modes of instability exist when $D < 0.247$, but when D is greater than this value, the maximum growth rate increases monotonically to the shear limit. Conversely, the maximum growth rate of the even mode decreases monotonically to the shear limit but, unlike the curve for the growth rate of the odd mode, there is an inflexion point at $D \simeq 0.05$. As we will demonstrate in our analysis

[2] By symmetry, the right-hand shear gives instabilities with the same phase speeds as the left-hand shear, and eigenfunctions of one type of shear will be reflections of the other.

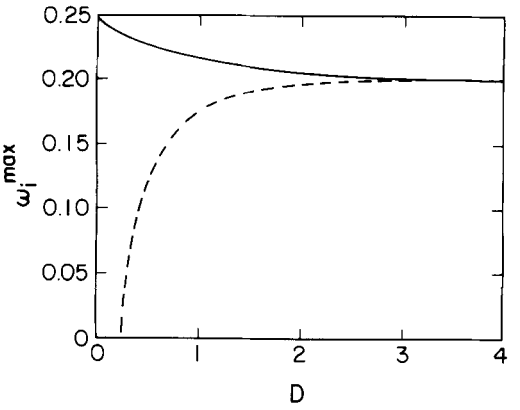

Figure 2 Temporal instability growth rates for a trapezoidal jet. The solid line corresponds to the even mode of instability and the dashed line corresponds to the odd mode.

of the smooth jet, an inflexion point is apparent in the curves of $\omega_i^{\max}$ corresponding to the even mode in stratified as well as unstratified fluid. The existence of an inflexion point is a subtle indication of the complex interactions that occur between the wave perturbation and the mean flow.

In our consideration of stratified symmetric jets, we assume the density to be exponentially decreasing with increasing z, *viz*: $\rho(z) = \rho_0 \exp(-\sigma\beta_0 z)$, where $\sigma\beta_0$ is constant. We define a smooth jet of width D by cleaving the Bickley profile in two and separating each section. Explicitly the velocity profile of the jet is represented by:

$$U_D(z) = \begin{cases} \operatorname{sech}^2(z + D), & z \leqslant -D, \\ 1, & -D \geqslant z \leqslant D, \\ \operatorname{sech}^2(z - D), & z \geqslant D. \end{cases} \tag{7}$$

In our analysis, we define a length scale so that D is measured in units of the half width at half maximum, $l = \cosh^{-1}(\sqrt{2})$. The shear profile on either side of the jet does not change as D increases, so the bulk Richardson number, which depends on the value of U_D' at the inflexion point, is independent of D.

As the jet becomes infinitely wide, the fluid motion is equivalent to two independent shear flows. Arbitrarily, we study the left-hand shear defined by

$$U_\infty(z) = \begin{cases} \operatorname{sech}^2 z, & z \leqslant 0, \\ 1, & z > 0, \end{cases}$$

which we will call a "Bickley shear". The temporal instability curves for various degrees of stratification of the shear flow are shown in Figure 3. Because, as discussed in Section 2, inaccuracies in the calculation of the growth rate arise for small α, such values are not shown.

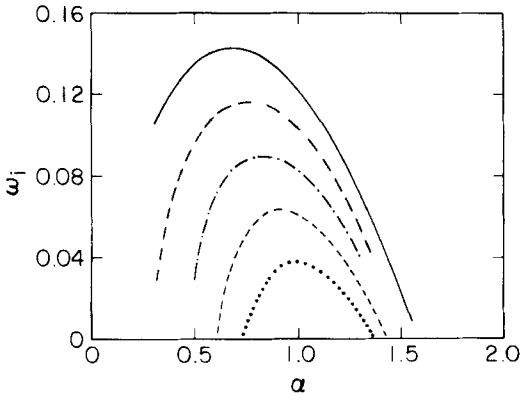

Figure 3 Temporal instability growth rates for a Bickley shear. The solid curve corresponds to unstratified flow. The other curves correspond to $N^2 = 0.025$ (large dash), $N^2 = 0.050$ (dash-dot), $N^2 = 0.075$ (small dash), and $N^2 = 0.1$ (dot).

Table 1 Maximum temporal instability growth rates for a Bickley shear

N^2	0.0	0.025	0.05	0.075	0.1	0.125
ω_i^{max}	0.1429	0.1165	0.0896	0.0630	0.0375	0.0136

As the stratification increases, the maximum growth rate ω_i^{max} decreases which reflects the stabilizing influence of stratified fluid. No unstable modes exist when $N^2 > 0.140$. Values of the maximum growth rates for increasing N^2 are listed in Table 1.

As D increases, the maximum growth rates of the even and odd modes asymptotically approach the corresponding growth rates of the shear limit. In Figure 4(a) and (b), we plot the difference of the maximum growth rate from the limit for both even and odd modes as a function of D. The five curves in each figure correspond to stratified fluid with $N^2 = 0.0, 0.025, 0.05, 0.075, 0.1$.

First we consider the MT modes of the unstratified jet. In this case, the growth rate of the MTO mode is a monotonically increasing function of D. Conversely, the growth rate of the MTE mode is not monotonic, rather it increases initially as D increases above zero and then decreases monotonically to the shear limit. Like the MTE mode of the trapezoidal jet, the curve has an inflexion point near $D = 0.3$ and for all D the even mode grows more quickly than the odd mode.

We begin our analysis of the instabilities in stratified jets by examining the variation in the growth rate of the MTE mode. When the Bickley jet ($D = 0$) is weakly stratified and $N^2 < 0.076$, the growth rate of the MTE mode is larger than the shear limit. When $0.076 < N^2 < 0.140$, the growth rate is smaller. In weakly stratified jets, therefore, the instability grows more rapidly when vortices that develop from one flank of the jet are strongly coupled to vortices from the other flank. The opposite

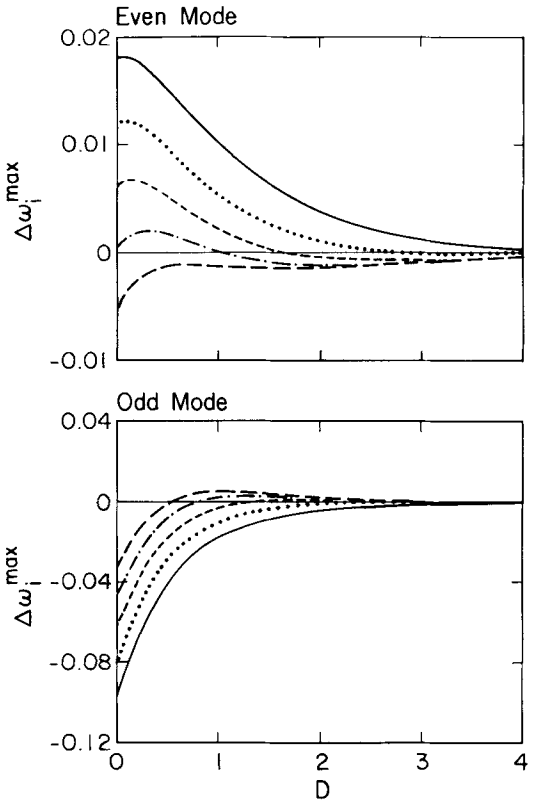

Figure 4 Difference from the shear limit of even and odd mode growth rates for a smooth jet of width D. In both figures, the solid curve corresponds to unstratified fluid. The other curves correspond to $N^2 = 0.025$ (dot), $N^2 = 0.050$ (small dash), $N^2 = 0.075$ (dash-dot), and $N^2 = 0.1$ (large dash).

is true in flows with a large degree of stratification: the instability is more unstable when the width of the jet is large and the vortices from each flank are weakly coupled. The curves are not monotonic; there is a tendency in all cases for the growth rate to increase initially as D increases.

We turn next to the study of the MTO mode which, as we have discussed, gives rise to the development of cores of opposite vorticity that grow adjacent to each other, For flows with any degree of stratification, the growth rate when $D = 0$ is smaller than the shear limit. In jets of larger width, for which there is a weaker interaction between adjacent vortex pairs, the mode becomes more unstable. With respect to the shear limit, the MTO modes are more unstable in highly stratified fluid than in fluid which is weakly stratified. A surprising result of our study is that, unless the jet is unstratified, ω_i^{max} becomes greater than the shear limit in a jet of large width. In particular, the MTO mode can actually grow faster than the MTE mode.

Though we have not performed a detailed investigation of the non-monotonicity

of the maximum growth rate, we believe this behaviour can be explained by over-reflection of neutrally propagating modes. A recent review of the over-reflection concept and an example of its application are provided in Smyth and Peltier (1989).

In order to gain some understanding of the underlying mechanism involved as the instabilities grow, we have studied the Reynolds stress and, in stratified fluid, the vertical density flux profiles for the MTE and MTO modes in the jet with widths $D = 0$ and $D = 0.5$. Each study is performed for unstratified fluid and for stratified fluid such that $N^2 = 0.05$. The wave parameters for these cases are given in Table 2. The Reynolds stress is defined by the product $\rho_0 \langle u'w' \rangle$ where the angle brackets indicate an average over one period in the horizontal direction and u' and w' are the horizontal and vertical components of the velocity perturbation, which can be calculated from derivatives of the streamfunction. This quantity is a measure of the transfer of horizontal momentum in the vertical direction. In particular, if $\tau(z)$ is the Reynolds stress, then the derivative $\tau'(z)$ is proportional to the rate at which the background flow will be accelerated by the growth of the instability. In a stratified jet, the vertical density flux, $\langle \rho'w' \rangle$, gives a measure of the mass transport by the mode; the z-derivative of $\langle \rho'w' \rangle$ is proportional to the rate at which heavier fluid is convected upwards or downwards by the instability.

The eigenfunction ϕ, which is used to calculate the Reynolds stress and vertical density flux, is normalized so that the magnitude of $\tau(z)$ equals unity at maximum. We define z_0 to be the vertical position of the maximum. (For the symmetric jet, another extremum of $\tau(z)$ occurs when $z = -z_0$.) In unstratified fluid, the extrema of $\tau(z)$ coincide with the inflexion points of the jet. Generally, $\tau(z)$ is greatest when z_0 is a zero of the imaginary part of η^2, defined in (2). Explicitly, z_0 satisfies

$$2N^2[U(z_0) - c_r] = U''(z_0)\{[U(z_0) - c_r]^2 + c_i^2\}. \tag{8}$$

When N^2 is small, this equation can be approximated by

$$2N^2 = U''(z_0)[U(z_0) - c_r]. \tag{9}$$

Table 2 Wave parameters of the MTE and MTO modes of a symmetric jet with width $D = 0.0$ and $D = 0.5$ in unstratified fluid and stratified fluid with $N^2 = 0.05$

Even mode:	$D = 0.0$		$D = 0.5$	
	$N^2 = 0.0$	$N^2 = 0.05$	$N^2 = 0.0$	$N^2 = 0.05$
α_r	0.9023	1.0311	0.7670	0.9330
c_r	0.4512	0.4788	0.4944	0.5255
ω_i	0.1608	0.0953	0.1579	0.0947
Odd mode:				
α_r	0.5179	0.5248	0.6789	0.6977
c_r	0.7154	0.7566	0.6529	0.6698
ω_i	0.0461	0.0268	0.1027	0.0718

In Figure 5a we show the Reynolds stress for unstratified flow. In all cases, we see that the momentum transfer decreases the strength of the shear. Therefore, the perturbation tends to stabilize the background flow and, in so doing, extracts kinetic energy from the background. The peaks in the profiles of the MTE and MTO modes in the unstratified jet coincide at the same vertical position as the inflexion points of the jet, specifically at $z_s \simeq 0.66$ for the jet of width $D = 0$. However, the form of the peaks of the MTE mode is markedly different from that of the MTO mode: whereas the stress profile of the MTE mode is large over an extended scale, that of the MTO mode is relatively localized. For a jet of width D, the profile of the Reynolds stress for each mode evolves to two distinct peaks which are separated by a domain of low stress whose extent equals D.

The stress profiles of the MT modes of the stratified jet with $N^2 = 0.05$ are shown in Figure 5b. The most notable effect of increasing the stratification is that the peaks of the Reynolds stress profile of the MTE and MTO mode no longer coincide with the inflexion points of the jet. For the jet of width $D = 0$, the peaks of the MTE mode occur further from the jet center at $z_0 \simeq 0.84$ and the peaks of the MTO mode occur closer to the jet center at $z_0 \simeq 0.56$. Both these results agree with equation (8)

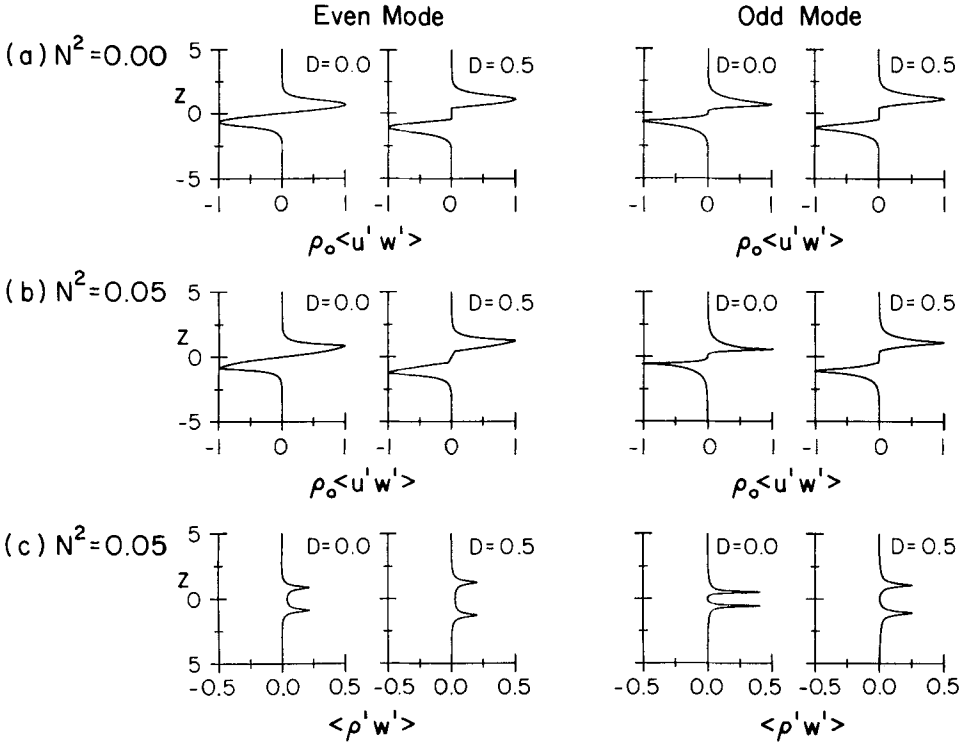

Figure 5 Profiles of Reynolds stress and vertical density flux for the MTE and MTO modes of a symmetric jet of width $D = 0$ and $D = 0.5$: (a) Reynolds stress for the unstratified jet, (b) Reynolds stress for the stratified jet with $N^2 = 0.05$, and (c) vertical density flux for the stratified jet with $N^2 = 0.05$.

for which the values of c are given in Table 2. The width of the peaks of the MTE mode does not change significantly when the jet is stratified, however, the peaks of the MTO mode tend to narrow. Hence the stress in the MTO mode becomes more localized.

The vertical density flux profiles of the MT modes of the stratified jet with $N^2 = 0.05$ are shown in Figure 5c. These are positive for all z which demonstrates that the instability tends to move dense fluid upward and so reduce the degree of stratification of the jet. The peaks of the MTO mode are narrower and more intense than those of the MTE mode and, in the MTO mode, there is no density flux at the center of the jet. Unlike the Reynolds stress profiles, the peaks of the MTO mode broaden as the jet width increases.

In summary, the MTE mode transfers momentum to reduce the strength of the shear in the jet more effectively than the MTO mode. The transport of momentum and mass by the MTO mode occurs over a smaller vertical scale. The greatest transport of momentum and mass in the MTE mode occurs farther from the center of the jet in stratified fluid than in unstratified fluid. In the MTO mode, this occurs closer to the center of the jet.

It remains to understand how the odd mode of instability can grow more quickly than the even mode in a sufficiently wide jet of stratified fluid. The solution may be found by an energy budget analysis in which we consider the temporal growth of perturbation energy as it changes due to the extraction of kinetic energy from the mean flow by the action of the Reynolds stress and the extraction of potential energy from the mean flow through the action of the perturbation vertical density flux. The relative contributions to the energy change by each is given by:

$$\frac{\partial}{\partial t}\langle E' \rangle_{xz} = \langle \rho_0 U' \langle u'w' \rangle_x \rangle_z - g\langle \rho' w' \rangle_{xz}, \tag{10}$$

where the brackets, $\langle\rangle_x$ and $\langle\rangle_z$, indicate horizontal and vertical averages, respectively, and

$$E' = \frac{1}{2}\rho_0(u'^2 + w'^2). \tag{11}$$

If the first term on the right hand side of (10) is dominant then the instability is dynamic, otherwise the instability is static. In Figure 6, we show the relative contributions of the extraction of kinetic energy and deposition of potential energy from/to the stratified mean flow with $N^2 = 0.05$ as a function of the jet width D. Both energy transfer terms are expressed as a fraction of twice the total kinetic energy of the instability. In this way we make use of the relationship,

$$\omega_i = \frac{1}{2\langle E' \rangle_{xz}}(\langle \rho_0 U' \langle u'w' \rangle_x \rangle_z - g\langle \rho' w' \rangle_{xz}), \tag{12}$$

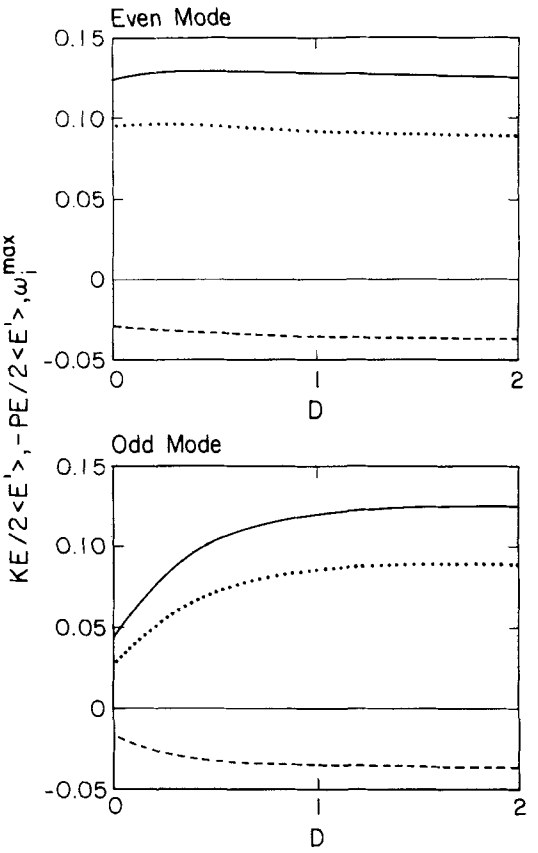

Figure 6 Energy analysis of the MTE and MTO modes in a symmetric jet of width D. The solid (dashed) line corresponds to the extracted kinetic (potential) energy. The dotted line is the sum of the two contributions which equals the growth rate ω_i. For comparison with the growth rate, values are normalized by twice the total kinetic energy of the instability.

so that the growth rate of the instability is expressed as the sum of contributions from kinetic energy extraction and potential energy deposition.

For both modes, but most notably for the MTO mode, we see that the maximum growth rate is larger in a jet of larger width primarily because the instability extracts kinetic energy from the mean flow more efficiently. The decrease of potential energy deposited to the mean flow by instabilities in jets of larger width is marginal in comparison.

For a stratified jet with $N^2 = 0.05$, the growth rate of the MTO mode becomes greater than the growth rate of the MTE mode when the jet width is approximately $D = 1.6$. At this width, the kinetic energy extracted by the MTO mode is comparable to the kinetic energy extracted by the MTE mode, however, because the perturbation is more localized about the shear zone, the deposited potential energy is smaller for the MTO mode than for the MTE mode. We conclude, therefore, that the MTO

mode grows more quickly than the even mode in a jet of large width because it extracts as much kinetic energy from the mean flow without depositing so much potential energy.

4. ABSOLUTE/CONVECTIVE INSTABILITY OF THE BICKLEY JET

In reality, not only does the mode of maximum growth rate dominate the initial stages of linear instability, but it is also affected by those modes with comparable wavenumber and growth rate. Together, the sum of these modes forms a wavepacket which travels with a real valued group velocity C. The analysis of the evolution of the wavepacket is closely connected with the theory of absolute/convective instability which we review below.

To fix ideas, it is sufficient to consider a one-dimensional wavepacket expressed as a composition of linear waves satisfying the dispersion relation $\omega = \omega(\alpha)$:

$$f(x,t) = \int_{-\infty}^{\infty} F(\alpha) \exp\{i[\alpha x - \omega(\alpha)t]\} d\alpha.$$

The long time evolution of the wavepacket observed from a frame of reference moving with speed $C = x/t$ is dominated by the growth of the mode with group velocity C. This can be demonstrated rigorously by application of the saddle point method such as that discussed in Copson (1965). Explicitly, as $t \to \infty$,

$$f(x,t) \simeq F(\alpha^*) \left\{ \frac{-2\pi i}{\left. \frac{d^2\omega}{d\alpha^2} \right|_{\alpha^*}} \right\}^{1/2} \frac{e^{i[c\alpha^* - \omega(\alpha^*)]t}}{t^{1/2}}, \tag{13}$$

where α^* is the, generally complex, wavenumber which corresponds to modes that move with group velocity

$$\left. \frac{d\omega}{d\alpha} \right|_{\alpha^*} = C. \tag{14}$$

The stability of the wavepacket travelling at this velocity is determined by the sign of its growth rate, $\mathrm{Im}[\omega(\alpha^*) - C\alpha^*]$.

The issue of absolute versus convective instability can be determined by considering the case where x is fixed as $t \to \infty$, so $C = x/t = 0$. The condition (14) therefore implies that there is a unique wavenumber α_0 corresponding to modes with zero group velocity; that is $\frac{d\omega}{d\alpha}|_{\alpha_0} = 0$. The stability of this mode is dictated simply by the sign of $\omega_i(\alpha_0)$: if $\omega_i(\alpha_0)$ is positive, the mode grows exponentially, eventually perturbing the entire flow, if $\omega_i(\alpha_0)$ is negative, the mode is damped so that any wavepacket

with zero group velocity is extinguished. The first kind of flow is said to be absolutely unstable. In flows of the second kind, all unstable modes have non-zero group velocity and so are ultimately swept away by the flow. Such flows are said to be convectively unstable.

From the Cauchy-Riemann relations, since ω is an analytic function of α, the complex derivative is

$$\frac{d\omega}{d\alpha} = \frac{\partial \omega_r}{\partial \alpha_r} + i\frac{\partial \omega_i}{\partial \alpha_r} = \frac{\partial \omega_i}{\partial \alpha_i} - i\frac{\partial \omega_r}{\partial \alpha_i}. \tag{15}$$

So the application of the condition that the group velocity is zero is equivalent to searching for what is typically a saddle-node of the function $\omega_i(\alpha)$. Note that the application of the saddle point method assumes that the saddle node, if not unique, has the largest value of $\mathrm{Im}[\omega(\alpha^*) - C\alpha^*]$ compared with other saddle-nodes. The complex dispersion relationship, like that shown in Figure 1, implies that a saddle-node, if it exists, is unique.

To ensure that the eigenvalue corresponding to α_0 lies on the manifold containing the known phase speeds for real α, a continuation method is used. In this method, the search for α_0 in the complex α plane begins with a real value of α for which the eigenvalue is well known. In each stage of the search, the value of α is incremented by small real and imaginary parts and the eigenvalue computed in one step is used as a first guess for the eigenvalue in the next step. In this way, if the increments are small enough, proper convergence is ensured by continuity of the eigenvalues. Provided the analytic function $\omega(\alpha)$ is slowly varying, the approximate position of the saddle node can be estimated by an extrapolation scheme such as the inverse parabolic method discussed in Section 2.

In general, we may consider the case where for all time $x/t = C$ is the speed of a moving frame of reference. Hence, we may examine the absolute/convective instability of the jet with respect to this frame, or equivalently, we may examine the stability characteristics of the mode which has group velocity C with respect to the rest frame. We say that the flow is absolutely unstable with respect to a moving reference frame of velocity C if the wavepacket which has group velocity C with respect to the stationary frame has positive growth rate, ω_i. Instabilities of a flow observed with respect to a reference frame moving at a speed C can be found by solving the Taylor-Goldstein equation in which the background velocity profile $U(z)$ is replaced by $U(z) - C$. However, the eigenvalue problem can be solved without integrating the equation with this replacement: if c is the phase speed of the instability in the stationary frame, then by taking advantage of the Galilean invariance of the Taylor-Goldstein equaton, the eigenvalue of the instability in the moving frame is given by $c - C$, and the corresponding frequency is $\omega^C = \alpha(c - C) = \omega - \alpha C$, where ω is the complex frequency observed in the stationary frame of the mode with the same wavenumber. Therefore, in this formalism, the mode that has group velocity C in the stationary frame has a wavenumber α_0 which corresponds to the saddle-node of $\omega^C(\alpha)$. This approach has the advantage that the continuation method can be used to scan the complex α-plane for the saddle node of ω^C as C varies.

In order to gain a better understanding of the evolution of a wavepacket composed of spatiotemporal modes of instability, we consider the evolution of a one dimensional gaussian pulse in a non-dispersive and a strongly dispersive flow. The amplitude of a gaussian pulse is given by the real part of

$$f(x,t) = e^{-x^2} e^{i\omega t}, \tag{16}$$

where, in a non-dispersive flow, ω satisfies the linear dispersion relation:

$$\omega = C(\alpha - \alpha_0) + \omega_0. \tag{17}$$

The (real) group velocity of the pulse in this flow is C. The Fourier transform of the space co-ordinate of the amplitude function gives

$$F(\alpha,t) = 2^{-1/2} e^{-\frac{1}{4}\alpha^2 + i\omega t}. \tag{18}$$

Substituting equation (17) into (18) and transforming back to real space, gives the time evolution of the wavepacket:

$$f(x,t) = \mathrm{Re}[e^{-(x-Ct)^2} e^{i(\omega_0 - C\alpha_0)t}]. \tag{19}$$

Therefore the wavepacket propagates uniformly with no dispersion. As it propagates, however, it oscillates with frequency $\mathrm{Re}[\omega_0 - C\alpha_0]$ and grows as $\mathrm{Im}[C\alpha_0 - \omega_0]$.

It is more realistic to examine wavepackets in a dispersive flow, a simple example of which satisfies the dispersion relation

$$\omega = -\tfrac{1}{2}r(\alpha - \alpha_0)^2 + C(\alpha - \alpha_0) + \omega_0. \tag{20}$$

Following the same procedure as before, we find that the real space time evolution of a gaussian wavepacket is given by

$$f(x,t) = \mathrm{Re}\{a \exp[i(-\tfrac{1}{2}r\alpha_0^2 - C\alpha_0 + \omega_0)t] \exp[-a^2(x - (C - r\alpha_0)t)^2]\}, \tag{21}$$

where

$$a = [1 + 2irt]^{-1/2}.$$

A gaussian pulse with group velocity C which is damped exponentially in time is shown in Figure 7a. The wavepacket is shown at times $t = 0.0$, 10.0, and 20.0. The parameters of the non-linear dispersion relation are $\omega_0 = 0.01 + i0.05$, $\alpha_0 = 1.0$, and $r = 0.1 + i0.1$. In Figure 7b, we show the evolution of an unstable wavepacket with the same parameters but here $\omega_0 = 0.01 - i0.05$. Although this pulse grows exponentially, it does not disturb the entire flow since its group velocity is positive. If we consider the evolution of the pulse as viewed from a reference frame moving with the same speed as the group velocity, we find that the wavepacket is given by

$$f(x,t) = \mathrm{Re}\{a \exp[i(\tfrac{1}{2}r\alpha_0^2 - C\alpha_0 + \omega_0)t] \exp[-a^2(x + r\alpha_0 t)^2]\}. \tag{22}$$

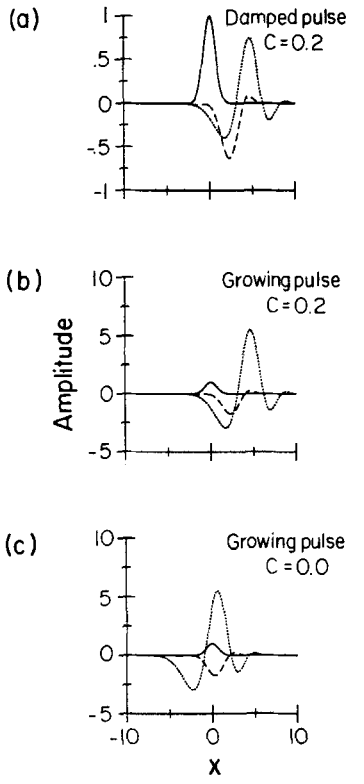

Figure 7 Evolution of gaussian wavepacket in a flow with quadratic dispersion relation at times $t = 0$ (solid line), 10 (dashed line), and 20 (dotted line): (a) exponentially damped wavepacket, (b) unstable, exponentially growing wavepacket, and (c) same unstable wavepacket as (b) viewed with respect to a frame of reference in which it has zero group velocity.

The evolution of the unstable gaussian pulse in a non-linear dispersive flow with the same parameters as above but viewed in the moving reference frame is shown in Figure 7c. In this frame, we see that the mode, whose relative group velocity is zero, eventually perturbs the entire flow.

We now prove that the wavenumber of the MC mode corresponds exactly with the wavenumber of the MT mode. First we show that the imaginary part of the wavenumber of the MC mode equals zero. If C is the group velocity of a pulse with respect to the stationary frame, then the growth rate of the pulse in the frame moving with speed C is $\omega_i{}^C = \omega_i - \alpha_i C$. From the Cauchy-Riemann relations, since C is real valued,

$$\frac{\partial \omega_r}{\partial \alpha_r} = \frac{\partial \omega_i}{\partial \alpha_i} = C \tag{23}$$

and

$$\frac{\partial \omega_i}{\partial \alpha_r} = -\frac{\partial \omega_r}{\partial \alpha_i} = 0. \tag{24}$$

For a given C, this pair of equations can be solved for a unique value of α (and hence ω). Therefore, α_r, α_i, ω_r, and ω_i can be thought of as functions of C.

Now, the condition that the growth rate as a function of C is a maximum for the MC mode at $C = C_0$ is

$$\left.\frac{d\omega_i^C}{dC}\right|_{C_0} = 0. \tag{25}$$

However,

$$\begin{aligned}\frac{d\omega_i^C}{dC} &= \frac{d\omega_i}{dC} - C\frac{d\alpha_i}{dC} - \alpha_i \\ &= \frac{\partial \omega_i}{\partial \alpha_r}\frac{d\alpha_r}{dC} + \frac{\partial \omega_i}{\partial \alpha_i}\frac{d\alpha_i}{dC} - C\frac{d\alpha_i}{dC} - \alpha_i \\ &= -\alpha_i.\end{aligned}$$

where (23) and (24) have been used to eliminate the terms involving partial derivatives. This result, combined with the condition of (25) shows that α is real-valued.

Next we show that the growth rate of the MC mode is maximum with respect to α_r. This follows from (24) and the result that $\alpha_i = 0$, since

$$\frac{\partial \omega_i^C}{\partial \alpha_r} = \frac{\partial \omega_i}{\partial \alpha_r} - \alpha_i\frac{\partial C}{\partial \alpha_r} = 0.$$

Because the MC mode and MT mode must satisfy the same conditions to be extrema, they must correspond to modes with the same wavenumber.

It is also a simple matter to prove that the group velocity of the most unstable spatial mode (MS) is real-valued. The MS mode corresponds to an absolute mode of instability with growth rate $-\alpha_i C_s$ in a frame moving with velocity $C_s = (\partial \omega_r/\partial \alpha_r) = (\partial \alpha_r/\partial \omega_r)^{-1}$.

Despite the growth in space of spatiotemporal modes, the temporal mode always dominates the initial stages of development of the non-linear dynamics of the flow. Consider, for example, the growth of a spatiotemporal mode which has wavenumber $\alpha = \alpha_r + i\alpha_i$ and frequency $\omega = \omega_r + i\omega_i$, and which travels with group velocity C. In the time t during which a wavepacket centered about this mode travels a distance x, the pulse is amplified by $\exp(-\alpha_i x + \omega_i t)$. But $x = Ct$ so the amplification is $\exp[(\omega_i - \alpha_i C)t] = \exp(\omega_i^C t)$. Therefore, the maximum growth rate of all

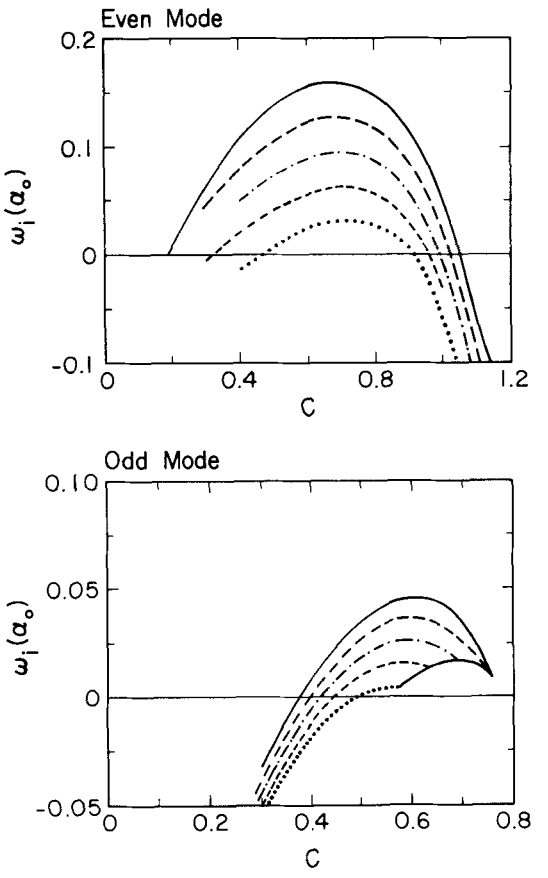

Figure 8 Growth rates of even and odd modes of instability with group velocity C. In both figures, the solid curve corresponds to unstratified fluid. The other curves correspond to $N^2 = 0.025$ (large dash), $N^2 = 0.050$ (dash-dot), $N^2 = 0.075$ (small dash), and $N^2 = 0.1$ (dot).

spatiotemporal modes is given by the largest value of ω_i^C, which, as we have shown, is the MC, or equivalently, the MT mode.

We have analyzed the absolute/convective instability of the Bickley jet by considering the growth rate of wavepackets as a function of the group velocity, C. The growth rate in flows with different degrees of stratification is plotted for even and odd modes in Figure 8. We have found, in accordance with Betchov and Criminale (1966), that the flow of an unstratified Bickley jet or wake is convectively unstable with respect to a stationary frame of reference. In this case, no saddle node of the function ω_i exists. Near the boundary between absolute and convective instability in weakly stratified fluid with low values of C, the determination of α_0 is difficult since the curvature of ω_i at the saddle node becomes infinite in one direction of the α-plane. Where convergence cannot be obtained, the growth rate is approximated by quadratic extrapolation of rates within the absolutely unstable region where the saddle-node

is well defined. Considering odd modes of instability in stratified flow for large values of C, it is possible that the imaginary part of the phase speed, c_i, may equal zero even when $\omega_i(\alpha_0)$ is positive and the flow is absolutely unstable. The boundary of marginal stability is indicated by the heavy line in Figure 8. We have verified that the maximum growth rates as a function of C of the even and odd modes correspond exactly to the growth rates of the MTE and MTO modes of the Bickley jet.

The boundary between absolute and convective instability regions for even and odd modes of the stratified Bickley jet is shown in Figure 9. This graph clearly shows the stabilization of the flow by stratification. Increasing the stratification decreases the range of C over which the flow is absolutely unstable. The odd modes are necessarily absolutely unstable when the even modes are unstable, though the converse is not true. The largest degree of stratification that allows absolute instability corresponds to the largest degree of stratification that allows temporal instability. This observation is a direct consequence of the equivalence of the MC and MT modes.

5. INSTABILITY OF A JET IN THE LEE OF TOPOGRAPHY

To provide an explanation for the origin of the severe downslope windstorm pulsations that are observed in association with the chinook of North America and the foehn of Switzerland, Scinocca and Peltier (1989) [see also Peltier and Scinocca (1990)] have studied non-linear computer simulations of inviscid, compressible, stratified flow over an idealized topographic obstacle. In the first cited paper, they were able to reproduce low altitude, high velocity wind pulsations from initial vertical profiles of horizontal velocity and potential temperature which were profiles recorded during the 11 January 1972 Boulder windstorm (which they denoted by "J11"). Simulations

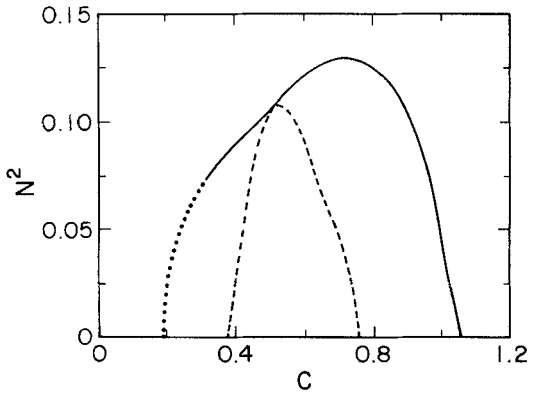

Figure 9 Regions of absolute and convective instability for even and odd modes of the Bickley jet. Solid (dashed) line corresponds to the boundary for even (odd) modes. Dotted lines indicate points of the curve derived by extrapolation. The area enclosed by each boundary indicates values of N^2 and C where the flow is absolutely unstable.

initialized with constant upstream velocity and Brunt-Väisälä frequency produced downstream behaviour which was remarkably similar to the J11 results, and so they concluded that the mechanism which gives rise to downstream pulsations does not depend sensitively on the details of the jet that develops in the lee of the topographic maximum. In order to further refine an understanding of the essential mechanism involved, an extensive study has recently been performed of the instabilities that develop from the flow described by the analytic solutions of Long's steady state, non-linear equations (Long, 1953). Details of the construction of Long's solution for flow over topography are provided by Laprise and Peltier (1989a) (see also Laprise and Peltier, 1989b; Laprise and Peltier, 1989c; Scinocca and Peltier, 1991).

Recent further work by Scinocca and Peltier (1991) has examined the non-linear evolution of the horizontal jet flow whose vertical profiles of velocity and potential temperature are defined by a vertical profile consisting of one wavelength of Long's solution above a critical position in the lee of the obstacle. Above this height, the velocity and Brunt-Väisälä frequency are defined to be constant so that the flow is rectified toward the far upstream ambient conditions. It has been verified by Scinocca and Peltier (1991) that such modifications do not strongly effect the dynamics of the instability in the shear zone of the jet. The profiles for the velocity and Brunt-Väisälä frequency squared extracted in this way from Long's solution are shown in Figure 10. The length and velocity scale are specified in dimensionless units so that the vertical extent of the domain is $L = 1.0$ and the maximum horizontal velocity is $V = 1.0$. In standard units, for comparison with the results of simulations by Scinocca and Peltier, the vertical extent of the domain is $L_* = 2048.5\,\text{m}$ and the maximum horizontal velocity is $v_* = 6.7475\,\text{m/s}$.

In our analysis of the temporal stability, we found modes of instability for wavenumbers in the range $0.0 \leqslant \alpha_r < 7.75$ (in dimensionless units) as shown in Figure 11. The MT mode has a wavenumber of 6.546 in dimensionless units, which in standard units corresponds to a wavelength of 2.00 km. This value agrees well with the wavelength of instabilities observed in the non-linear simulations.

The wave parameters of the MT mode are given in Table 4. This mode is particularly interesting since it is not localized to the region about the shear zone of the jet, rather it is a radiating mode. In particular, for large values of z the Reynolds stress profile of the mode, shown in Figure 12, is positive and decreases gradually. Therefore, kinetic energy which is extracted from the mean flow is propagated upward. This effect occurs because the Brunt-Väisälä frequency is large compared to the wavenumber of the disturbance, and so, according to equations (1) and (2), as z increases the streamfunction is not strongly damped but is of the form of weakly damped oscillations with damping of order c_i.

Also in Figure 12, we compare the Reynolds stress and vertical density flux profiles of the MT mode with the temporal modes whose growth rates are half as large (denoted by LT and HT for the modes with lower and higher wavenumber respectively). We see in the Reynolds stress profiles that less kinetic energy is propagated upward in disturbances of large wavenumber. Focusing on the Reynolds stress profile for the MT mode in the shear zone of the jet, we see that it is characterized by two strong negative peaks indicating that this mode acts strongly to reduce the

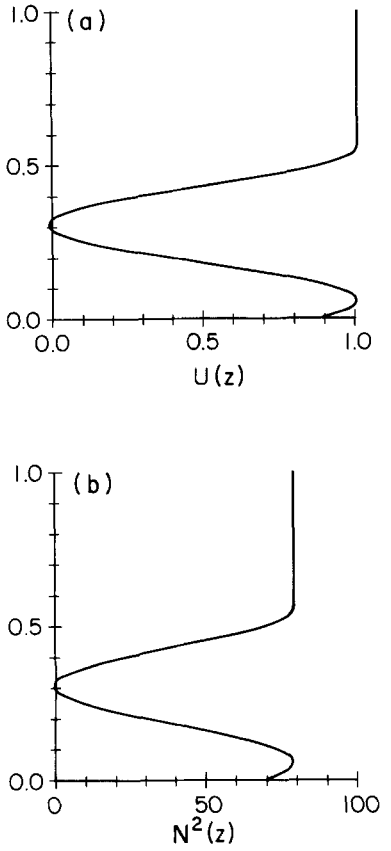

Figure 10 Profiles of (a) horizontal velocity and (b) Brunt-Väisälä frequency squared for a lee-averaged jet formed by a topographic obstacle.

shear on each flank of the jet. The LT and HT modes reduce the shear on one flank of the jet while the shear on the other flank is only weakly reduced. The vertical density flux profiles show that there is negligible mass transport outside the shear zone of the jet. The MT mode transports denser fluid upward from below and above the jet, and in the center of the jet, where N^2 is negative, denser fluid is transported downward.

We perform an energy budget analysis using equation (10). However, an extra term, $\langle p'w' \rangle_x|_{zmax}$, representing the positive energy flux through the upper boundary is subtracted from the right hand side. In this way we found that the growth rate agreed to within 0.1 percent of the growth rate determined by the eigenvalue. By comparing values of the energy contributions of the Reynolds stress, vertical density flux, and the flux of energy out of the upper boundary as in Table 3, we see that the dominant factor in the growth of the MT mode is a combination of the relatively large amount of kinetic energy which is extracted by reducing the shear on each flank

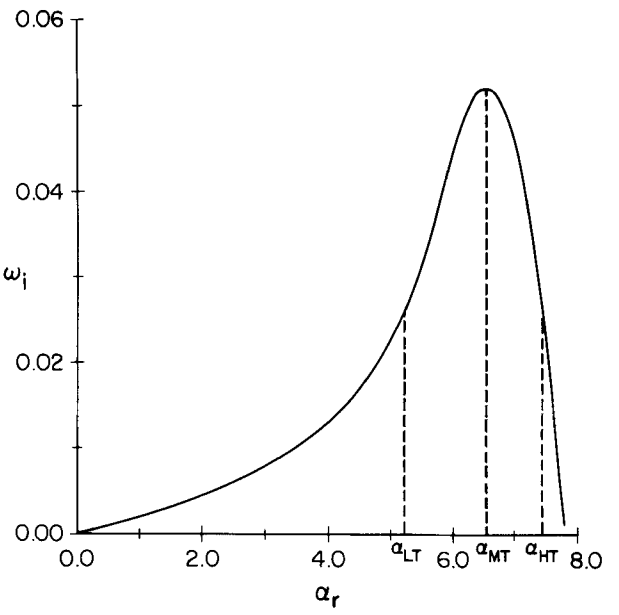

Figure 11 Growth rates versus wavenumber of temporal mode of instability for jet in lee of a topographic obstacle. Indicated are the wavenumbers corresponding to the MT mode and to the modes with half its growth rate.

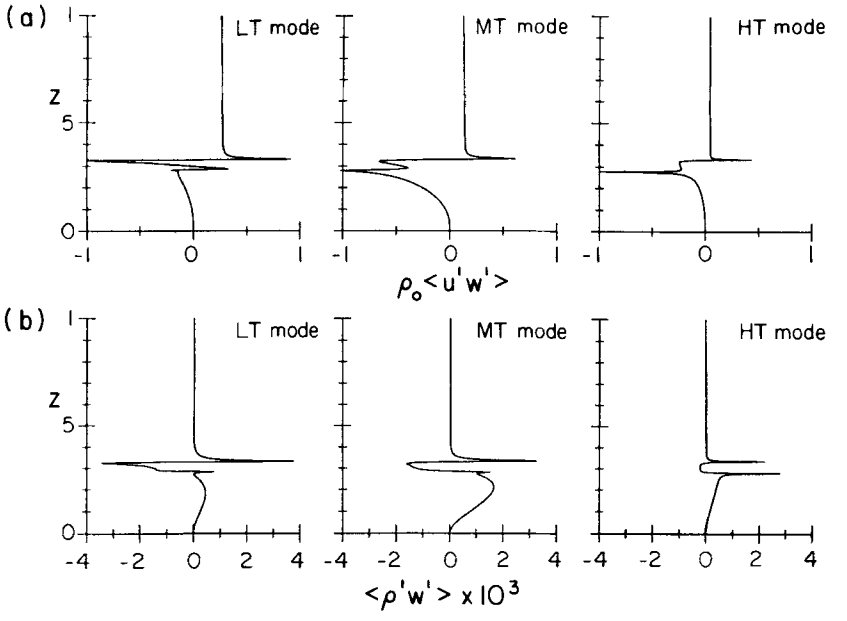

Figure 12 (a) Reynolds stress and (b) vertical density flux profiles for the MT mode and for modes LT and HT, which grow at half its rate.

Table 3 Energy contributions to the growth rate of the LT, MT, and HT modes normalized by twice the total perturbation energy of the mode

Mode	*Reynold's stress*	*Vertical density flux*	$\langle P'w' \rangle\|_{zmax}$	ω_i
LT	0.144	−0.010	−0.109	0.026
MT	0.139	−0.044	−0.043	0.052
HT	0.091	−0.031	−0.034	0.026

Table 4 Wave parameters for the MT, MS, and C0 modes with respect to a stationary frame of reference

Wave parameters	*MT mode*	*MS mode*	*CO mode*
α_r	6.546	3.130	0.468
α_i		−3.235	−4.279
ω_r	0.0439	0.0093	0.0057
ω_i	0.0521		−0.0016
c_r	0.00671	0.00144	0.00088
C	0.05364	0.00265	0.00037

of the jet and the relatively small amount of energy which is radiated outward in this mode. In the table, energy is normalized by a factor $2\langle E' \rangle$ so that each column is expressed as a contribution to the growth rate ω_i of each mode.

In Figure 13 we show the streamlines $\psi + \varepsilon\psi'$ of the flow due to the instability $\psi' = \mathrm{Re}\{\phi(z)\exp(i\alpha x)\}$ of the MT mode. In the figure, the perturbation parameter $\varepsilon = 0.1$ and ψ' is normalized to have a maximum value of 1. Consistent with observations by Scinocca and Peltier we observe a mode with structure qualitatively similar to the odd mode of a symmetric jet. That is, eddies with opposite vorticity develop so that they are situated almost adjacent to each other. In a symmetric jet, the growth of an odd mode would be observed though its domination over the even mode would not depend on the jet width as discussed in Section 3, rather, the even mode would be suppressed entirely in any case due to the fixed lower boundary condition.

A linear stability analysis of the (spatial) growth rates of spatial modes of instability shows that there is a mode with a well defined maximum growth rate and for which the wavenumber is significantly different from the MT mode. The frequency of the MS mode is indicated in Figure 15 which shows the growth rate α_i of spatial modes as a function of ω_r. The MS spatial growth rate is large, nonetheless the mode grows slowly compared to the MT mode since, as we show below, the group velocity of the wavepacket centered about the MS mode is small.

We look more closely now at wavepackets which evolve in the jet. In Figure 16 we show the growth rates of modes with zero group velocity observed in a frame moving with velocity C. The MS and MT modes are indicated by the modes with group velocity C_s and C_t respectively. When C is larger than the small critical value $C_0 \simeq 0.000374$, the flow is absolutely unstable. Due to the sensitivity of the numerical analysis, the upper bound of the absolutely unstable region could not be determined.

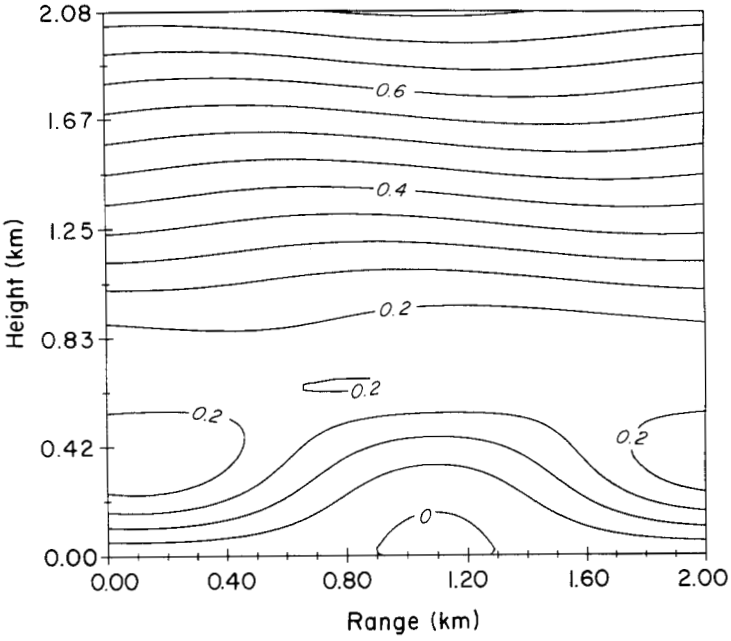

Figure 13 The streamfunction of the jet perturbed by the MT mode (perturbation parameter is $\varepsilon = 0.1$). Note that the eddies of opposite vorticity are positioned almost adjacent to each other.

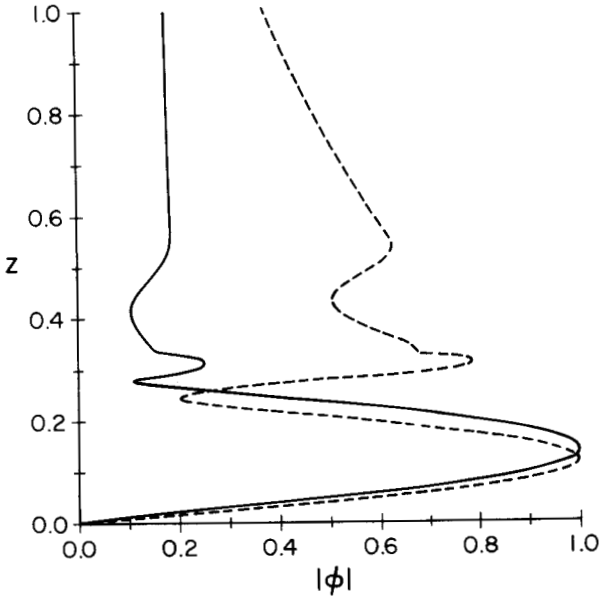

Figure 14 The norm of the streamfunction amplitude for the MT (solid line) and MS (dashed line) modes.

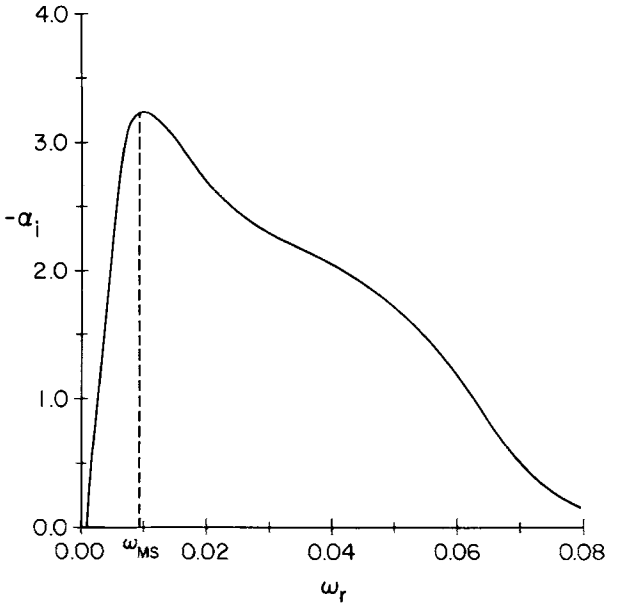

Figure 15 The growth rate of spatial modes of instability of the jet as a function of frequency. The frequency of the MS mode is indicated.

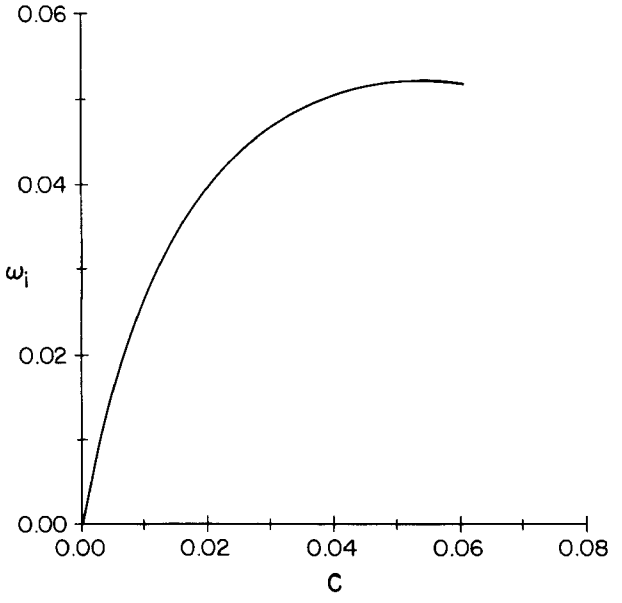

Figure 16 The growth rate of modes with zero group velocity observed in a moving frame of speed C with the flow.

Values of the MS wave parameters are compared with the MT mode in Table 4. For completeness, we also include in the table the wave parameters corresponding to the mode with group velocity C_0, which we call the C0 mode. All values, including those for the C0 mode, are given with respect to the stationary reference frame. We determine relative growth rates of the spatial and temporal modes by comparing $\omega_i^{C_s} = -C_s\alpha_i \simeq 0.0086$ of the MS mode with $\omega_i^{C_t} = \omega_i \simeq 0.052$ of the MT mode. Since the growth rate of the MS mode is an order of magnitude smaller than the temporal mode, it should not be seen directly in observations. Nonetheless, it may be possible to observe some dynamics in the spatial mode since the magnitude of the perturbation in the MS mode is two to three times greater than the MT mode at high altitudes. The magnitude of the stream function amplitude for both MT and MS modes are shown in Figure 14. For both modes, the stream function is normalized so that $|\phi| = 1$ at maximum. The group velocity of the MT mode, $C_t \simeq 0.0536$, is consistent with the unstable mode observed in the non-linear simulations of Scinocca and Peltier (1991).

6. CONCLUSION

We have shown that even and odd modes of instability in a symmetric jet undergo non-trivial modifications as the jet widens. The maximum growth rate of the even modes is larger than the growth rate of odd modes when $D = 0$ since it extracts much more kinetic energy from the mean flow than the kinetic energy extracted by the odd mode. At larger jet widths the kinetic energy extracted by both modes becomes comparable; however, the potential energy deposited by the odd mode is smaller than that deposited by the even mode since the odd mode is more localized about the shear maxima. Since the mode of maximum growth determines the ensuing non-linear dynamics, it is crucial to have a good understanding, not only of the wavelength and phase speed, but of the parity of the mode involved. In order to present an accurate description of the full non-linear development of vortices in each mode, an analysis of the instabilities of viscous flow should be performed. We have initiated such a program of analysis.

We have shown, for a stratified flow, which relative velocities will admit absolutely unstable behaviour in the Bickley jet. The range of relative velocities decreases as the degree of stratification increases. By understanding under which conditions a flow is convectively or absolutely unstable, experimentalists may be able to interpret their results more effectively. Presently, the issue of absolute versus convective instability in a jet flow is relevant to many analyses that concern the growth of linear modes and their effect upon the ensuing non-linear behaviour. We have given a practical example of such an analysis by studying the linear instabilities that develop in the shear zone of an idealized asymmetric stratified jet that is created by a topographic obstacle. In non-linear simulations where instabilities are excited by noise over a small horizontal range, one might expect to observe the growth only of spatial modes. This is not the case, however, as we confirm by a linear stability analysis; the downstream evolution of the MS mode is obscured by the development

of a faster growing wavepacket. In agreement with non-linear simulations, we have shown that the fastest growing mode of instability is the temporal mode. The wavelength and group velocity of the MT mode predicted by our linear stability analysis correspond well with the simulations. Furthermore, the structure of this mode, which is qualitatively similar to the odd mode of instability in a symmetric jet, is consistent with simulations, and has the surprising feature that it radiates energy upward, well away from the shear zones of the jet. If downslope windstorms do indeed radiate energy upward in this manner, indirect experimental observations may be made many kilometers above their surface manifestation.

Acknowledgements

The authors would like to thank Larry Pratt whose comments were extremely useful in developing the final draft of this paper.

References

Bers, A., "Theory of absolute and convective instabilities," *International Congress: Waves and Instabilities in Plasmas,* Inst. Theoret. Phys., Innsbruck, Austria (1973).

Betchov, R. and Criminale, W. O., "Spatial instability of the inviscid jet and wake," *Phys. Fluids* **9** (2), 359–362 (1966).

Bickley, W. G., "The plane jet," *Phil. Mag.* **23** (7), 727–31 (1937).

Briggs, R. J., *Electron-stream Interaction with Plasmas.* Cambridge M.I.T. Press, Boston (1964).

Copson, E. T., *Asymptotic expansions,* Cambridge University Press, Cambridge (1965).

Drazin, P. G. and Howard, L. N., "Hydrodynamic stability of parallel flow of inviscid fluid," *Advances in Applied Mathematics* **9** 1–89 (1966).

Drazin, P. G. and Reid, W. H., *Hydrodynamic Stability,* Cambridge University Press, Cambridge (1981).

Flierl, G. R., Stern, M. E. and Whitehead, J. A., "The physical significance of modons. Laboratory experiments and general integral constraints," *Dyn. Atmos. Oceans* **7**, 233–263 (1963).

Gaster, M., "A note on the relation between temporally-increasing and spatially-increasing disturbances in hydrodynamic stability," *J. Fluid Mech.* **14**, 222–224 (1962).

Hazel, P., "Numerical studies of the stability of inviscid stratified shear flows," *J. Fluid Mech.* **51**, 39–61 (1972).

Heurre, P. and Monkewitz, P. A., "Absolute and convective instabilities in free shear layers," *J. Fluid Mech.* **159**, 151–168 (1985).

Laprise, R. and Peltier, W. R., "The linear stability of nonlinear mountain waves: Implications for the understanding of severe downslope windstorms," *J. Atmos. Sci.* **46** (4), 545–564 (1989a).

Laprise, R. and Peltier, W. R., "On the structural characteristics of steady finite-amplitude mountain waves over bell-shaped topography," *J. Atmos. Sci.* **46** (4), 486–495 (1989b).

Laprise, R. and Peltier, W. R., "The structure and energetics of transient eddies in a numerical simulation of breaking mountain waves," *J. Atmos. Sci.* **46** (4), 565–585 (1989c).

Lin. S.-J. and Pierrehumbert, R. T., "Absolute and convective instability of inviscid stratified shear flows," *Proceedings of the Third International Symposium on Stratified Flows,* Cal. Inst. Tech., Pasadena, Cal., (1987).

Long, R. R., "Some aspects of the flow of stratified fluids. A theoretical investigation," *Tellus* **5**, 42–58 (1953).

Marcus, P. S., "Vortex dynamics in a shearing zonal flow," *J. Fluid Mech.* **215**, 393–430 (1990).

Miles, J. W., "On the stability of heterogeneous shear flows," *J. Fluid Mech.* **10**, 496–508 (1961).

Muller, D. E., "A method for solving algebraic equations using an automatic computer," *Mathematical Tables and Aids to Computation,* **10**, 208–215 (1956).

Overman, E. A. and Zabusky, N. J., "Evolution and merger of isolated vortex structures," *Phys. Fluids* **25**, 1297–1305 (1962).

Peltier, W. R. and Scinocca, J. F., "The origin of severe downslope windstorm pulsations," *J. Atmos. Sci.* **47** (24), 2853–2870 (1980).

Sato, H., "The stability and transition of a two-dimensional jet," *J. Fluid Mech.* **7**, 53–80 (1960).

Sato, H. and Kuriki, K., "The mechanism of transition in the wake of a thin flat plate placed parallel to a uniform flow," *J. Fluid Mech.* **11**, 321 (1961).

Scinocca, J. F. and Peltier, W. R., "Pulsating downslope windstorms," *J. Atmos. Sci.* **46**, 2885–2914 (1989).

Scinocca, J. F. and Peltier, W. R., Submitted to *J. Atmos. Sci.* (1992).

Sharp, P. W. and Fine, J. M., *User guide for ERNY: An explicit Runge-Kutta Nystrom integrator for second order initial value problems,* University of Toronto, Department of Computer Science (1987).

Smyth, W. D. and Peltier,W. R., "The transition between Kelvin-Helmholtz and Holmboe instability: An investigation of the overreflection hypothesis," *J. Atmos. Sci.* **46** (24), 3698–3720 (1989).

Sommeria, J., Meyers, S. D. and Swinney, H. L., "Laboratory simulations of Jupiter's great red spot," *Nature* **331**, 689–693 (1988).

Zabusky, N. J. and Deem, G. S., "Dynamical evolution of two-dimensional unstable shear flows," *J. Fluid Mech.* **47**, 353–379 (1971).